

Cite this: *Nanoscale*, 2011, **3**, 2868

www.rsc.org/nanoscale

PAPER

One-dimensional extended lines of divacancy defects in graphene

A. R. Botello-Méndez,^{*a} X. Declerck,^a M. Terrones,^b H. Terrones^a and J.-C. Charlier^a

Received 2nd November 2010, Accepted 28th December 2010

DOI: 10.1039/c0nr00820f

Since the outstanding transport properties of graphene originate from its specific structure, modification at the atomic level of the graphene lattice is needed in order to change its electronic properties. Thus, topological defects play an important role in graphene and related structures. In this work, one-dimensional (1D) arrangement of topological defects in graphene are investigated within a density functional theory framework. These 1D extended lines of pentagons, heptagons and octagons are found to arise either from the reconstruction of divacancies, or from the epitaxial growth of graphene. The energetic stability and the electronic structure of different *ideal* extended lines of defects are calculated using a first-principles approach. *Ab initio* scanning tunneling microscopy (STM) images are predicted and compared to recent experiments on epitaxial graphene. Finally, local density of states and quantum transport calculations reveal that these extended lines of defects behave as quasi-1D metallic wires, suggesting their possible role as reactive tracks to anchor molecules or atoms for chemical or sensing applications.

1. Introduction

Graphene, the one-atom-thick 2D allotrope of carbon, is a potential candidate for several technological applications.^{1,2} In particular, its outstanding structural and electronic properties make graphene an attractive material for constructing future nanoelectronics devices.³ However, graphene cannot be integrated as a building block for pure carbon-based field effect transistor devices due to the lack of a good $I_{\text{on}}/I_{\text{off}}$ ratio associated to the absence of an energy gap. Instead, electronic confinement, achieved by cutting the 2D plane into narrow (< 5 nm) 1D graphene nanoribbons (GNRs), is needed to create such a gap in the vicinity of the Fermi energy.^{4,5} Other strategies consisting in inducing a mobility gap in the GNRs *via* either chemical functionalization⁶ or doping have also been proposed.⁷

Since the outstanding transport properties of graphene originate from its specific structure, modification at the atomic level of the graphene lattice is needed in order to change its electronic properties. Indeed, topological defects, defined as the introduction of non-hexagonal rings in the carbon lattice preserving the connectivity of the network, play a very important role in graphene and related nanostructures.⁸ From a purely geometrical viewpoint, the inclusion of pentagons in an otherwise perfect

honeycomb lattice leads to a loss of 60° , inducing positive curvature. On the other hand, a heptagonal ring introduces an excess of 60° , thus creating a saddle point in the honeycomb lattice. Therefore, pentagon-heptagon pairs, such as those formed in a Stone-Thrower-Wales (STW) defect^{9,10} (where a single carbon-carbon bond is rotated 90°) can preserve the planarity of graphene. In fact, the creation of large domains composed only of pentagons and heptagons instead of hexagons is indeed possible.^{11,12,13} Recent experiments on ion-irradiated graphene also suggest that lattice defects can be considered as a potential source of intervalley scattering, which could in principle transform graphene from a metal into an insulator,¹⁴ thus controlling its electronic structure.

Grain boundaries (GB) can be considered as a way to introduce lattice defects in a controlled manner. Atomic resolution scanning tunneling microscopy (STM) studies of GB in graphite have often been interpreted as lines of heptagonal and pentagonal defects.¹⁵ More recently, a bottom-up approach was used to create an extended line of defects (ELD) in graphene.¹⁶ In this experiment, two graphene half-sheets were grown epitaxially with two different arrangements on a nickel substrate, inducing an atomic translation relative to each other. Due to this difference, when the two halves merge at the boundary, they are naturally reconstructed through topological defects. The authors suggested that the fingerprints observed in their STM images are caused by an array of defects containing octagonal and pentagonal carbon rings embedded in a perfect graphene sheet. In addition, their electronic structure calculations confirm that the proposed one-dimensional carbon defect possessed a density of states that is reminiscent of the metallic edge states observed in graphene flakes.¹⁶

^aUniversité Catholique de Louvain, Institute of Condensed Matter and Nanosciences, Place Croix du Sud 1 (NAPS-ETSF-Boltzmann), 1348, Louvain-la-Neuve, Belgium. E-mail: andres.botello@uclouvain.be

^bThe Exotic Nanocarbon Research Center (JST), Shinshu University, Wakasato 4-17-1, Nagano, 380-8553, Japan, and Department of Physics & Materials Research Institute, The Pennsylvania State University, University Park, PA 16802-6300, USA

Using a first-principles approach, the present work explores various architectures of ELDs embedded in graphene, exhibiting pentagonal, heptagonal and octagonal rings of carbon. Three different stable atomic configurations are predicted to arise from the reconstruction of periodic divacancies. *Ab initio* simulated STM images are also predicted in order to help the identification of such ordered arrays of defects within experimental observations. Finally, electronic structure and quantum transport calculations are performed on these 1D arrays of defects embedded in graphene nanoribbons (GNRs) in order to predict their quasi-1D metallic-wire behavior, thus suggesting new properties for pure-carbon nanoelectronic devices.

2 Reconstruction from divacancies

Different divacancy defects with various orientations relative to the zigzag direction could be formed (Fig. 1). A first option consists of removing carbon dimers oriented perpendicularly to the zigzag chains (Fig. 1(a)). It is expected intuitively that after geometrical relaxation, the structure would be composed of two pentagons separated by an octagon, also perpendicular to the zigzag orientation. However, the energy needed to achieve such a large strain prevents the octagons from being formed. Instead, a C–C bond rotation (STW) is needed to relieve the strain, as illustrated by the d5d7 structure in Fig. 1(a). The second option consists of removing the carbon dimers tilted 30° from the zigzag orientation, resulting in an alternated series of octagons and two pentagons sharing a same side, as represented with the 585 structure in Fig. 1(b). A less strained 585 structure could be obtained by displacing one of the two graphene domains connected to the GB by $\frac{1}{2}a$, where a is the lattice parameter of

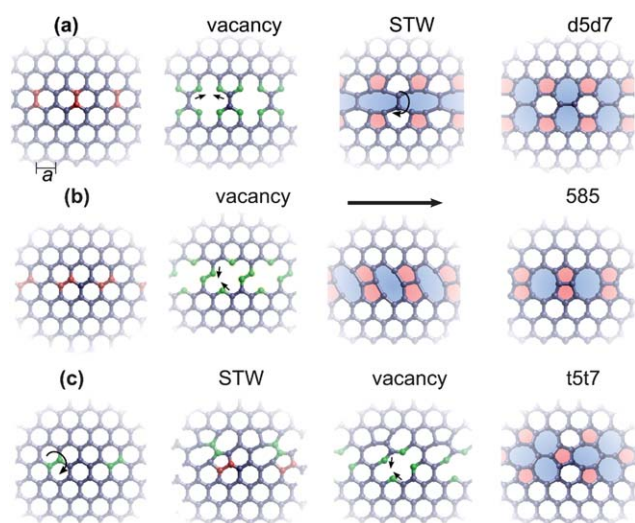


Fig. 1 Formation of different extended lines of defects in graphene through the reconstruction of divacancies. Lines of defects are formed after the removal of carbon dimers (in red), either (a) perpendicular or (b) with a 30° deviation from the zigzag direction. These extended arrays of defects are called (a) d5d7 (double-5 double-7 structure) and (b) 585 (pentagon-octagon-pentagon structure), respectively. Further displacement of one graphene side by $\frac{1}{2}a$ (black arrow in b) is required to relax the 585 grain boundary as observed in Ref. [16]. An extended array of defects composed of a series of three pentagons and three heptagons (t5t7- triple-5 triple-7 structure) is also topologically possible when the divacancy reconstruction occurs along with a STW transformation (c).

graphene. Such a GB structure is the one observed during the epitaxial growth of graphene¹⁶ (Fig. 1(b)). An alternative array of defects could be reconstructed from divacancies by means of a STW transformation, thus leading to a triple-pentagon triple-heptagon (t5t7) structure as depicted in Fig. 1(c). Such a defect shape has already been suggested as a stable topology for the reconstruction of an isolated divacancy in graphene.¹⁷

3 Calculation details

The energetic stability and the ground-state properties of these lines of defects, arising from the reconstruction of divacancies are investigated using the density functional theory (DFT)^{18,19} as implemented in the SIESTA code,²⁰ under the local spin-density approximation (LSDA)²¹ and generalized gradient approximation (GGA)²² for the exchange correlation functional. Using this DFT formalism, the *ab initio* calculations were performed on ideal graphene and on lines of defects embedded in graphene. When the array of defects is introduced, a minimal distance of ~ 22 Å is present between the ELDs, and periodic boundary are used to ensure 20 Å of vacuum between slabs. In order to deal with the large number of atoms in the supercell, norm-conserving pseudo-potentials²³ and a numerical localized combination of atomic orbitals (double- ζ basis) to expand the wave-functions are used. The energy levels are populated using a Fermi–Dirac distribution with an electronic temperature of 250 K and an energy cutoff of 500 Ry is used. The integration over the 2D Brillouin zone is replaced by a summation over a regular grid of 32×6 k -points (or equivalent k -point density). The geometries are fully relaxed until the forces on each atom and stress tolerance are less than 0.005 eV Å⁻¹ and 0.005 GPa, respectively. In addition, calculations were also performed on large hydrogenated zigzag GNRs with 15 zigzag chains (15zGNR) along its width (~ 33 Å), and ~ 11 Å separation between the various 1D array of defects and the edges.

4 Results and discussion

4.1 Formation energies

The formation energy²⁴ per C-atom involved in the ELD reconstruction ($E_c(\alpha)$) can be calculated as follow:

$$E_c(\alpha) = (E_T(\alpha) - (N_\alpha - \eta_\alpha)E_{gr}) / \eta_\alpha - E_{gr} \quad (1)$$

where α indicates the nature of the ELD: d5d7, 585, or t5t7, so that $E_T(\alpha)$ is the total energy of a graphene plane containing a α -type line of defects. N_α and η_α stand for the total number of atoms in the unit cell, and the atoms involved in the reconstruction of the divacancies to form the ELD. E_{gr} is the energy per C atom in perfect graphene. Consequently, $E_c(\alpha)$ is an estimation of the amount of energy required (e.g. through thermal excitation) to achieve the reconstructions; however, the relative stability is difficult to address, since the number of atoms to form each reconstruction (η_α) is different. A more general cohesive energy per unit of length ($E'_c(\alpha)$) can be introduced as:

$$E'_c(\alpha) = (E_T(\alpha) - N_\alpha E_{gr}) / d_\alpha \quad (2)$$

where d_α is the cell parameter in the direction of the ELD.

While LDA calculations tend to underestimate the lattice parameters of graphene, GGA calculations tend to overestimate these values. Therefore, upper and lower limit values could be obtained for the formation energies of these defective systems. Both energies (E_c and E_c'), with both approximations are summarized in Table 1. LDA calculations predict that the most stable reconstruction of an array of divacancies is a line of t5t7 defects (see Fig. 1(c)), whereas the GGA calculations predict that the most stable reconstruction is the 585 array of defects. Note that the experimental observation of the 585 reconstruction is constrained by the synthesis conditions as described above.¹⁶ However, in a top down approach, *e.g.* vacancy creation through irradiation, the reconstruction would be either with the t5t7 or d5d7 line of defects, and would be most probably driven by the kinetics and interaction with the substrate. It is noteworthy that the LDA prediction of the stability of the t5t7 ELD is consistent with previous calculations performed on isolated defects in graphene and carbon nanotubes carried out with a plane wave basis set and a GGA functional.¹⁷

It has been shown that isolated defects could induce wave-like buckling of the graphene sheet.²⁵ To investigate this, we have carried out calculations of the extended lines of defects with a slight out of plane perturbation as a starting point. The optimized structure indeed exhibits some buckling. In contrast with the isolated defect, the buckled extended line of defects is less stable than the planar one. This is an indication that the strain on the C–C bonds is better accommodated in a planar extended line of defects than in an isolated defect.

4.2 STM simulation

STM constitutes an excellent experimental tool for identifying defects in graphene.²⁶ However, the interpretation of STM images can be complicated, and the use of simulated images is crucial. Therefore, in order to help in the identification of such

Table 1 Formation energies per atom (E_c) and per unit of length (E_c') for lines of defects embedded in graphene. Energy differences between the anti-ferromagnetic ($E_{\uparrow\downarrow}$) and the ferromagnetic ($E_{\uparrow\uparrow}$) spin orientations at the edges of a 15zGNR containing extended lines of defects (ELDs) centered in the middle of its width

α -ELD	E_c^{LDA} (eV atom ⁻¹)	$E_c'^{\text{LDA}}$ (eV Å ⁻¹)	E_c^{GGA} (eV atom ⁻¹)	$E_c'^{\text{GGA}}$ (eV Å ⁻¹)	$E_{\uparrow\downarrow} - E_{\uparrow\uparrow}$ (meV)
d5d7	0.264	0.760	0.415	0.145	-0.72
585	0.258	0.527	0.270	0.133	-1.93
t5t7	0.171	0.512	0.691	0.231	5.94

ELD, STM images have been calculated from the *ab initio* local density of states (LDOS) of defects embedded in GNRs using the Tersoff-Hamann approximation (Fig. 2). LDOS are computed between 0.2–0.3 eV with respect to the Fermi energy (*i.e.* $E_F = 0$) in order to account for an n-type doping substrate, *e.g.* Ni or Au.²⁷ It is noteworthy that the simulated images for the 585 ELD (Fig. 2(b)) exhibit a good agreement with the experimental STM image reported in Ref. [16], which was taken at 100mV.

4.3 Electronic and quantum conductance properties

In order to verify the potential advantages of these 1D arrays of defects in nanoelectronics, spin-polarized band structures and transport calculations were carried out for each of the three ELDs embedded in a 15zGNR. For each configuration, energy bands appear close to the Fermi energy, allowing extra channels to the conductance in these 1D systems (Fig. 3). Perfect zigzag GNRs exhibit a ferromagnetic ($\uparrow\uparrow$) coupling along the edges, but an antiferromagnetic ($\uparrow\downarrow$) coupling between the edges.²⁸ This inter-edge coupling opens a band gap for zigzag GNRs with small width. The introduction of the ELD might screen the interaction between the edge states. The difference between the $\uparrow\downarrow$ and $\uparrow\uparrow$ spin configurations for the pristine 15zGNR is ~ -2.9 meV. This energy difference slightly decreases when a 585 or d5d7 line of defects is introduced (see Table 1). Although in the error range of DFT calculations, such a weak inter-edge coupling suggests that the two spin configurations are equally probable. In contrast, the ferromagnetic orientation ($\uparrow\uparrow$) is clearly favored for the t5t7 ELD, thus inducing an unexpected *always-metallic* GNR.

Fig. 4 displays the spin polarized quantum conductance for the three defected 15zGNRs, calculated using the Landauer formalism, and the surface Green's function matching method, after extracting the first-principles Hamiltonian and overlap matrices.^{29,30} Note that, in particular, the t5t7 line of defects introduce extra conduction channels, and can thus be considered as one-dimensional metallic wires embedded into a GNR. This result is consistent with the STM images and clearly demonstrates the presence of localized states extended along the 1D array of defects parallel to the ribbons axis.

A top-down approach to achieve these lines of defects could consist of modifying the graphene surface at the atomic scale and thereby controlling the topological disorder. Indeed, either electron beam irradiation,³¹ or scanning tunneling lithography^{32,33} could be used to induce and manipulate vacancies in graphene. The low migration energy of single vacancies³⁴ facilitates their coalescence into divacancies. Under high

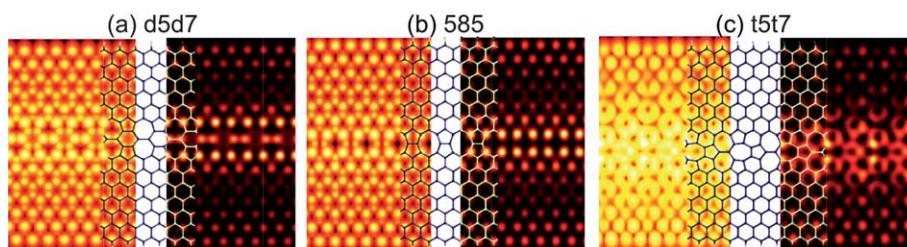


Fig. 2 *Ab initio* STM images simulated at (left) constant current ($6.7 \times 10^{-4} e/\text{\AA}^3$) and (right) constant height (10.6 Å) for the (a) d5d7, (b) 585, and (c) t5t7 extended lines of defects.

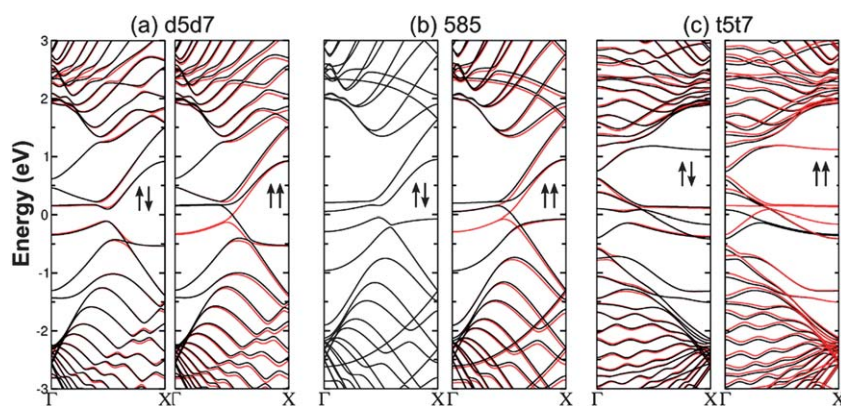


Fig. 3 Spin-polarized band structures for the (a) d5d7, (b) 585, and (c) t5t7 extended lines of defects embedded in a zigzag nanoribbon with either an anti-parallel ($\uparrow\downarrow$) or a parallel ($\uparrow\uparrow$) spin-configuration at the edges.

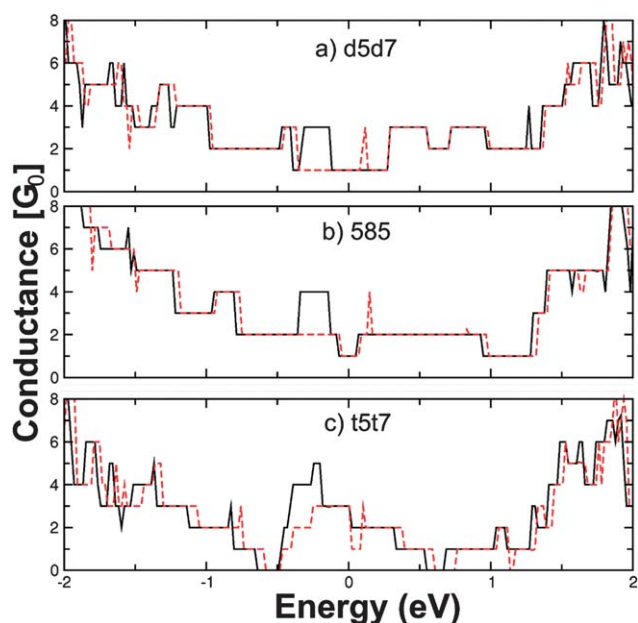


Fig. 4 Spin-polarized quantum conductances (up: black down: red) for (a) d5d7, (b) 585 and (c) t5t7 ELD in a 15zGNR.

concentration of divacancies, the short range motion of the reconstructed defects,³⁵ lead to aligned reconstructions at high temperatures.³⁶ An ordered reconstruction upon heat treatment could thus create different types of extended lines of defects between graphene domains with the same orientation, as illustrated in Fig. 1(a) and (c). However, the controlled formation of grain boundaries that occur between boundaries of graphene with different orientation^{16,37,38} seems more difficult to control because of the complex kinetics involved during epitaxial growth.

5 Conclusion

In summary, 1D extended lines of defects exhibit localized states along the line and behave like metallic wires embedded in graphene sheets. We present lower and upper limit values for the formation energies of three different kinds of lines of defects that could arise from the reconstruction of divacancies. In particular,

the t5t7 ELD induces extra conduction channels and localized states which could enhance the chemical reactivity of graphene. This extended defect opens the possibility of arranging molecules or atoms in a linear fashion, thus behaving as a 1D template. Such atomic-scale carbon-based wires could have a big impact on the future development of smaller functional devices.

6 Acknowledgements

J.-C. C. and X. D. acknowledge financial support from the F.R.S.-FNRS of Belgium. A. R. B. M. is indebted to the *M. De Merre* Prize of Louvain. H. T. acknowledges support from the Ecole Polytechnique of Louvain, where he is a visiting professor. M. T. from the Japan Regional Innovation Strategy Program by the Excellence, JST. Parts of this work are directly connected to the Belgian PAI6 Program and to the NANOHYMO ARC project.

References

- 1 K. S. Novoselov, A. K. Geim, S. V. Morozov, D. Jiang, Y. Zhang, S. V. Dubonos, I. V. Grigorieva and A. A. Firsov, *Science*, 2004, **306**, 666–669.
- 2 A. K. Geim and K. S. Novoselov, *Nat. Mater.*, 2007, **6**, 183–191.
- 3 H. C. Neto, F. Guinea, N. M. R. Peres, K. S. Novoselov and A. K. Geim, *Rev. Mod. Phys.*, 2009, **81**, 109–54.
- 4 Y. Son, M. L. Cohen and S. G. Louie, *Phys. Rev. Lett.*, 2006, **97**, 216803–4.
- 5 S. M. Dubois, Z. Zanolli, X. Declerck and J. Charlier, *Eur. Phys. J. B*, 2009, **72**, 1–24.
- 6 A. López-Bezanilla, F. Triozon, S. Latil, X. Blase and S. Roche, *Nano Lett.*, 2009, **9**, 940–944.
- 7 A. Lherbier, X. Blase, Y. Niquet, F. Triozon and S. Roche, *Phys. Rev. Lett.*, 2008, **101**, 036808.
- 8 H. Terrones and A. Mackay, *Carbon*, 1992, **30**, 1251–1260.
- 9 A. Stone and D. Wales, *Chem. Phys. Lett.*, 1986, **128**, 501–503.
- 10 P. A. Throver, *Chem Phys Carbon*, 1969, **5**, 217–319.
- 11 V. H. Crespi, L. X. Benedict, M. L. Cohen and S. G. Louie, *Phys. Rev. B: Condens. Matter*, 1996, **53**, R13303.
- 12 H. Terrones, M. Terrones, E. Hernández, N. Grobert, J. Charlier and P. M. Ajayan, *Phys. Rev. Lett.*, 2000, **84**, 1716.
- 13 M. T. Lusk and L. D. Carr, *Phys. Rev. Lett.*, 2008, **100**, 175503.
- 14 J. Chen, W. G. Cullen, C. Jang, M. S. Fuhrer and E. D. Williams, *Phys. Rev. Lett.*, 2009, **102**, 236805.
- 15 P. Simonis, C. Goffaux, P. Thiry, L. Biro, P. Lambin and V. Meunier, *Surf. Sci.*, 2002, **511**, 319–322.
- 16 J. Lahiri, Y. Lin, P. Bozkurt, I. I. Oleynik and M. Batzill, *Nat. Nanotechnol.*, 2010, **5**, 326–329.

-
- 17 R. G. Amorim, A. Fazio, A. Antonelli, F. D. Novaes and A. J. R. da Silva, *Nano Lett.*, 2007, **7**, 2459–2462.
 - 18 P. Hohenberg and W. Kohn, *Phys. Rev.*, 1964, **136**, B864.
 - 19 W. Kohn and L. J. Sham, *Phys. Rev.*, 1965, **140**, A1133.
 - 20 J. M. Soler, E. Artacho, J. D. Gale, A. Garcia, J. Junquera, P. Ordejon and D. Sanchez-Portal, *J. Phys.: Condens. Matter*, 2002, **14**, 2745–2779.
 - 21 D. M. Ceperley and B. J. Alder, *Phys. Rev. Lett.*, 1980, **45**, 566.
 - 22 J. P. Perdew, K. Burke and M. Ernzerhof, *Phys. Rev. Lett.*, 1996, **77**, 3865.
 - 23 N. Troullier and J. L. Martins, *Phys. Rev. B: Condens. Matter*, 1991, **43**, 1993.
 - 24 S. Boys and F. Bernardi, *Mol. Phys.*, 2002, **100**, 65.
 - 25 J. Ma, D. Alfé, A. Michaelides and E. Wang, *Phys. Rev. B: Condens. Matter Mater. Phys.*, 2009, **80**, 033407.
 - 26 H. Amara, S. Latil, V. Meunier, P. Lambin and J. Charlier, *Phys. Rev. B: Condens. Matter Mater. Phys.*, 2007, **76**, 115423.
 - 27 M. Vanin, J. J. Mortensen, A. K. Kelkkanen, J. M. Garcia-Lastra, K. S. Thygesen and K. W. Jacobsen, *Phys. Rev. B: Condens. Matter Mater. Phys.*, 2010, **81**, 081408.
 - 28 H. Lee, Y. Son, N. Park, S. Han and J. Yu, *Phys. Rev. B: Condens. Matter Mater. Phys.*, 2005, **72**, 174431.
 - 29 V. Meunier and B. G. Sumpter, *J. Chem. Phys.*, 2005, **123**, 024705–8.
 - 30 E. Cruz-Silva, F. López-Urías, E. Muñoz-Sandoval, B. G. Sumpter, H. Terrones, J. Charlier, V. Meunier and M. Terrones, *ACS Nano*, 2009, **3**, 1913–1921.
 - 31 J. A. Rodríguez-Manzo and F. Banhart, *Nano Lett.*, 2009, **9**, 2285–2289.
 - 32 L. Tapasztó, G. Dobrik, P. Lambin and L. P. Biro, *Nat. Nanotechnol.*, 2008, **3**, 397–401.
 - 33 F. Banhart, J. Kotakoski and A. V. Krasheninnikov, *ACS Nano*, 2011, **5**, 26–41.
 - 34 A. Krasheninnikov, P. Lehtinen, A. Foster and R. Nieminen, *Chem. Phys. Lett.*, 2006, **418**, 132–136.
 - 35 O. Cretu, A. V. Krasheninnikov, J. A. Rodríguez-Manzo, L. Sun, R. M. Nieminen and F. Banhart, *Phys. Rev. Lett.*, 2010, **105**, 196102.
 - 36 G.-D. Lee, C. Z. Wang, E. Yoon, N.-M. Hwang, D.-Y. Kim and K. M. Ho, *Phys. Rev. Lett.*, 2005, **95**, 205501.
 - 37 O. V. Yazyev and S. G. Louie, *Phys. Rev. B: Condens. Matter Mater. Phys.*, 2010, **81**, 195420.
 - 38 O. V. Yazyev and S. G. Louie, *Nat. Mater.*, 2010, **9**, 806–809.